3URFHHGLQJVRIWKHWK,QWHUQDWLRQDO+HDW7UDQVIHU&RQIHUHQ
,7&
6HSWHPEHU:DVKLQJWRQ&86$

NANO-STRUCTURED TWO-PHASE HEAT SPREADER FOR COOLING ULTRA-HIGH HEAT FLUX SOURCES

Mitsuo Hashimoto
Sony corporation
Shinagawa-ku, Tokyo, Japan

Hiroto Kasai
Sony corporation
Shinagawa-ku, Tokyo, Japan

Kazuma Usami
Sony corporation
Shinagawa-ku, Tokyo, Japan

Hiroyuki Ryoson
Sony corporation
Shinagawa-ku, Tokyo, Japan

Kazuaki Yazawa
UC Santa Cruz
Santa Cruz, CA, USA

Justin A. Weibel
Purdue University
West Lafayette, IN, USA

Suresh V. Garimella
Purdue University
West Lafayette, IN, USA

ABSTRACT

A two-phase heat spreader has been developed for cooling high heat flux sources in high-power lasers, high-intensity light-emitting diodes, and semiconductor power devices. The heat spreader targets the passive cooling of heat sources with fluxes greater than 5 W/mm^2 without requiring any active power consumption for the thermal solution. The prototype vapor chamber consists of an evaporator plate, a condenser plate and an adiabatic section, with water as the phase-change fluid. The custom-designed high heat flux source is composed of a platinum resistive heating pattern and a temperature sensor on an aluminum nitride substrate which is soldered to the outside of the evaporator. Experiments were performed with several different microstructures as evaporator surfaces under varying heat loads. The first microstructure investigated, a screen mesh, dissipated 2 W/mm^2 of heat load but with an unacceptably high evaporator temperature. A sintered copper powder microstructure with particles of 50 μm mean diameter supported 8.5 W/mm^2 without dryout. Four sets of particle diameters and different thicknesses for the sintered copper powder evaporators were tested. Additionally, some of the sintered structures were coated with multi-walled carbon nanotubes (CNT) that were rendered hydrophilic. Such nano-structured evaporators successfully showed a further reduction in thermal resistance of the vapor chamber.

INTRODUCTION

Energy-efficient thermal management solutions are being continually explored for high-performance electronic devices. Fan and heat sink-based air convection systems are commonly used in consumer electronics applications but their performance is limited. Single-phase and two-phase active liquid cooling systems are receiving increased interest in order to meet the steady growth in performance specifications. For devices such as high power lasers or concentrator photovoltaic systems, such liquid-cooling methods provide a practical solution; however, the extra power required to pump fluid through these systems is a prohibitive factor for most consumer electronics applications.

The development of a new passive cooling technology that can manage high heat fluxes with low manufacturing and assembly costs is highly desired. Currently, vapor chambers are widely used as passive cooling devices. Commercially available devices support approximately 1 W/mm^2 (1) of heat flux. Zhao *et al.* (2), (3) developed a bi-dispersed wick structure which achieved a cooling rate of 3.3 W/mm^2. Various wick microstructures have been studied and reported in the literature, both in terms of detailed experimental investigations and analytical modeling efforts (4-17). While a few passive cooling devices offer heat dissipation levels approaching 3.5 W/mm^2, this is insufficient for managing the high heat dissipation sources of interest in this study. One

possible enhancement technique towards improving performance is through the use of high conductivity, large surface area CNTs within the evaporator structure. CNTs have been previously shown to enhance boiling heat transfer (18-21). Integrating such a nano-structured surface onto conventional microstructure wicks to improve thermal performance is the motivation of this study. In a similar study, Cai *et al.* (22) developed a patterned CNT array evaporator surface that was shown to support 6 W/mm^2 but the surface was not incorporated into an operating device.

The goal of the present work is to develop a two-phase heat spreader capable of removing greater than 5 W/mm^2 of heat flux from a device, and to experimentally demonstrate its performance. In a recent precursor to this study (23), conventional screen mesh and sintered copper wick structures were explored by the authors. In the present work, more detailed experiments are conducted, along with the incorporation of CNTs into the wick structures.

DESIGN OF THE HEAT SPREADER

A prototype heat spreader device is designed and fabricated to allow for the testing of multiple evaporator surface designs, as shown in Fig. 1.

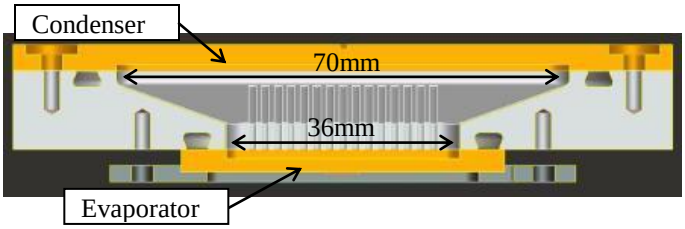

Fig. 1 Cross-sectional diagram of the prototype heat spreader.

The heat spreader is designed to be inserted into a thermal stack as a flat plate. The top surface serves as a condenser and the lower surface as an evaporator. The interior walls seal to the top and bottom plate to create a closed chamber and provide a fluid return path from condenser to evaporator. The walls are made from stainless steel and are insulated during testing such that they can be assumed to be adiabatic. To provide a large enough condensing area and liquid return path to test the evaporation performance, a screen mesh is attached to the condenser plate by diffusion bonding.

The components were designed so that a heat dissipation level of more than 5 W/mm^2 could be accommodated, according to the requirement that the pressure loss caused by vapor and liquid flow resistance must be smaller than the capillary pressure provided by the evaporator.

$$\Delta P_{eva,cap} \geq \Delta P_{loss} = \Delta P_{eva,l} + \Delta P_{adi,l} + \Delta P_{con,l} + \Delta P_{con,cap}$$

Each term is calculated assuming a 5 W/mm^2 heat input.

The pressure drop in the screen mesh along the condenser and the inclined adiabatic region surfaces (#30 mesh screen), as well as that along the evaporator surface (24) is estimated from

$$\Delta P_{x,l} = \frac{\mu_l \dot{m}_l L}{A \rho_l K}.$$

The capillary pressure drop in the condenser is given by

$$\Delta P_{x,cap} = \frac{2\sigma \cos\theta}{r_{eff}}$$

The chosen screen mesh was thus verified to provide the required feeding flow.

Fig. 2 shows a photograph of the prototype heat spreader. The tube visible on the side is used for evacuating air, filling working fluid, and draining excess liquid.

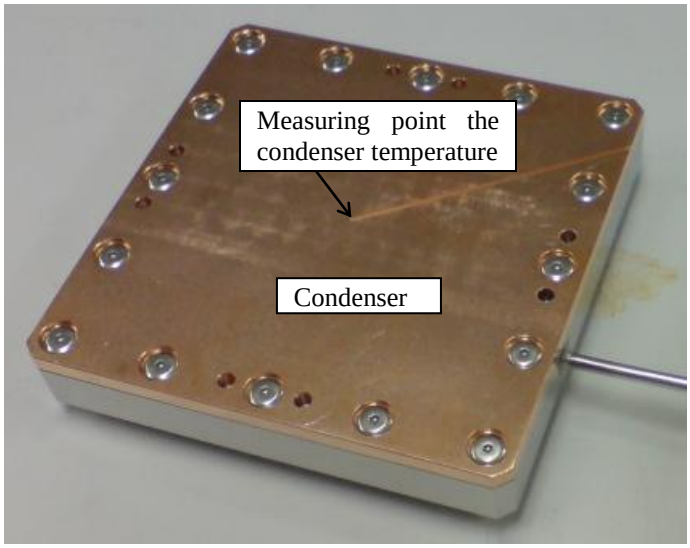

Fig. 2 Photograph of the assembled heat spreader.

EXPERIMENTAL SETUP & SAMPLE PREPARATION

The experiments for this work require a concentrated heat source that produces extremely high heat fluxes of greater than 5 W/mm^2. A heat source is custom-designed and fabricated for this purpose. A 1 μm thick patterned platinum film is deposited onto a 200 μm thick aluminum nitride substrate as shown in Fig. 3. The electrical resistance of the heater as fabricated is 120 Ω. Another pattern incorporated at the center of the heater to sense the temperature-dependent electrical resistance *in situ*. This chip is soldered to the exterior surface of the evaporator using an 80%Au 20%Sn solder (melting temperature 278 °C). The lead wires powering the heat source are shown in Fig.4.

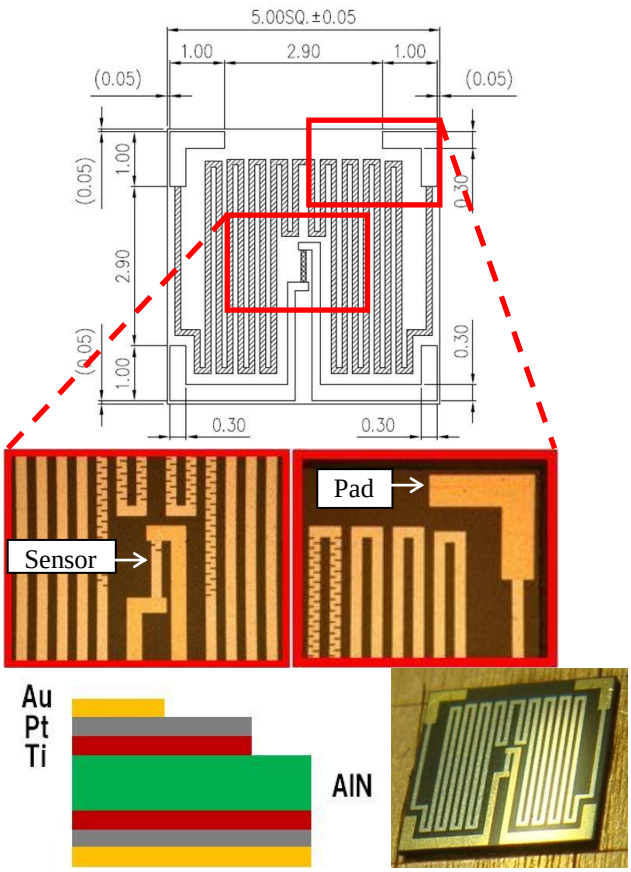

Fig. 3 Detail of the heat source: plan view and cross-section of the layered structure.

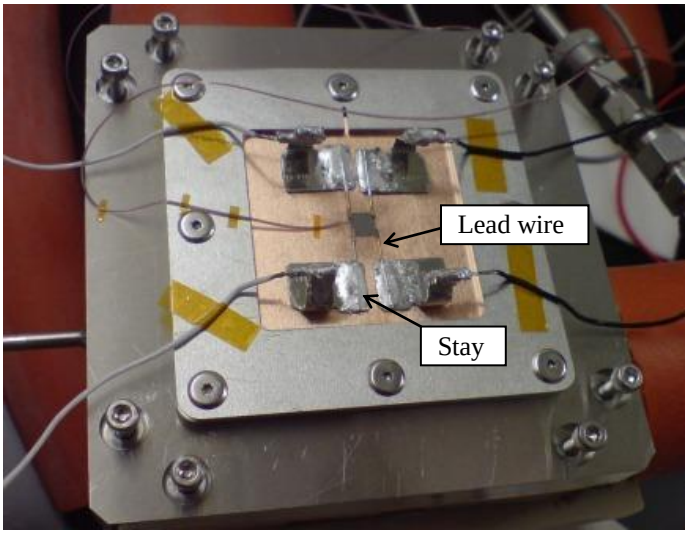

Fig. 4 Image of the back side of the heat spreader showing the heat source.

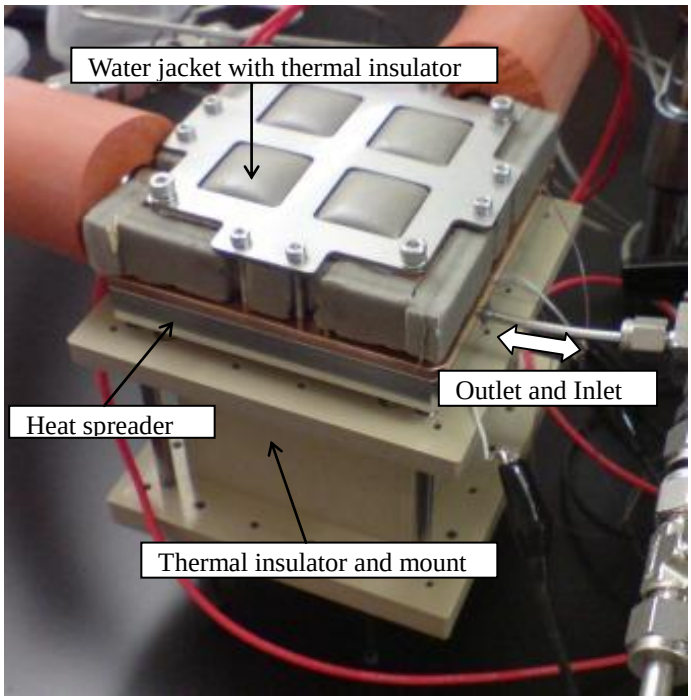

Fig. 5 Image of the assembled experimental setup.

The exterior surface of the condenser plate is attached to a water-cooling jacket for ultimate heat removal from the device. The interface between the jacket and plate is filled with thermal grease to maximize the thermal conductance. The condenser temperature is maintained at approximately 40 °C (an acceptable temperature for consumer products) by controlling the fluid inlet and outlet temperature.

Fig. 5 shows the test setup assembly including the cooling jacket and insulation. The liquid filling process is performed after mounting the water-cooling jacket on the assembly to eliminate any mechanical damage due to the otherwise dramatic pressure changes that may occur. This process begins by purging air from the chamber followed by charging pure water up to full capacity. The amount of water and the inside pressure are then reduced in small steps by heating. The optimum amount of charge varies depending on the applied heat flux, and therefore, different amounts of charge were used for individual test samples. Excess working liquid degrades the heat transfer coefficient for both evaporation and condensation.

Both screen mesh and sintered powder wick samples are prepared as shown in Fig. 6. The screen mesh evaporator was attached to the oxygen-free copper substrate by diffusion bonding. To sinter powder on to the oxygen-free copper substrates, a sintering process was performed in a furnace at 950 °C in an argon atmosphere (25). Four variants of sintered evaporators were prepared and one of them is shown in Fig. 6 as an example.

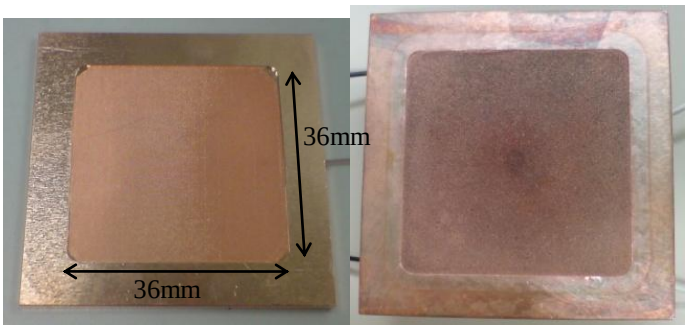

Fig. 6 Screen mesh evaporator (left) with mesh number #200 and thickness 0.1 mm, and sintered copper powder evaporator (right) with particle diameter 50 μm and thickness 1.5 mm.

For the nanostructured samples, CNTs were deposited onto the sintered copper substrate by thermal chemical vapor deposition. A catalyst layer is prepared by two different methods: by sputtering three layers of Fe/Al /Al_2O_3 onto the particles, and using a dendrimer catalyst. The dendrimer solution serves to coat the surface with nanoparticle catalyst due to its unique repeatedly branched molecular structure (26, 27). Thus, the dendrimer catalyst helps to control the CNT geometry and density. Both growth methods are investigated to verify uniform coverage of CNT growth and secure anchoring to the surface. The characteristics of each CNT evaporator are shown in the next section.

CNTs are commonly known to be hydrophobic as fabricated, an undesirable characteristic for an evaporator. It is a critical requirement to have a low-contact-angle, wetting evaporator. The CNT samples are exposed to ultraviolet wave irradiation (28) prior to testing, which renders the CNTs hydrophilic. This occurs due to the oxidization of carbon which allows hydrogen coupling with water.

TEST RESULTS AND DISCUSSION

The performance dependence of the device on the different evaporator surfaces fabricated is characterized. Effects of the microstructure are first explored, followed by those of the CNT parameters.

The superheat temperature is defined as the difference between the temperature at the heat source thermal sensor and the temperature of the condenser plate. The condenser temperature is measured with a thermocouple mounted on the center of its exterior surface.

Effects of Wick Microstructure – Mesh & Sintered Powder

Fig. 7 shows that the screen mesh evaporator supports slightly above 2 W/mm^2 of heat flux. Heat fluxes greater than 2.1 W/mm^2 could not be tested since the resulting temperature exceeded the melting point of the solder (and not because a dryout condition was reached). The superheat temperature was 185 °C at 2 W/mm^2. In any case, this superheat is excessive for electronics cooling applications.

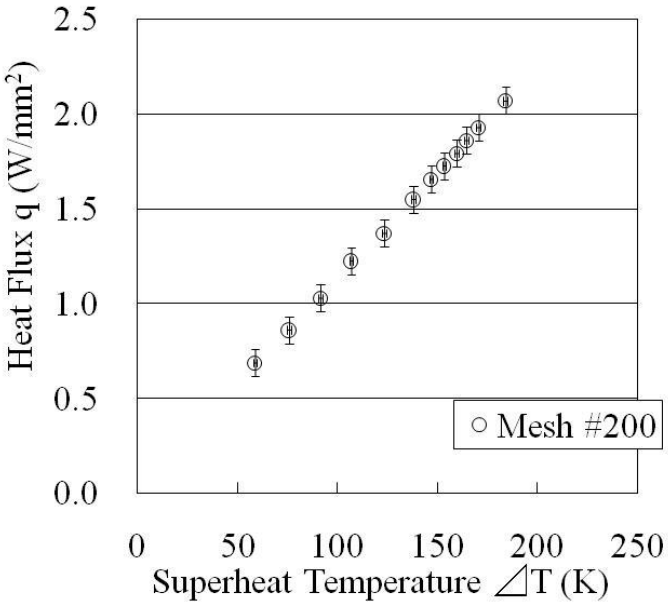

Fig. 7 Thermal performance of the screen mesh evaporator. The test was stopped at a heat flux of 2.1 W/mm^2 not due to a dryout condition but since the melting point of the solder was reached.

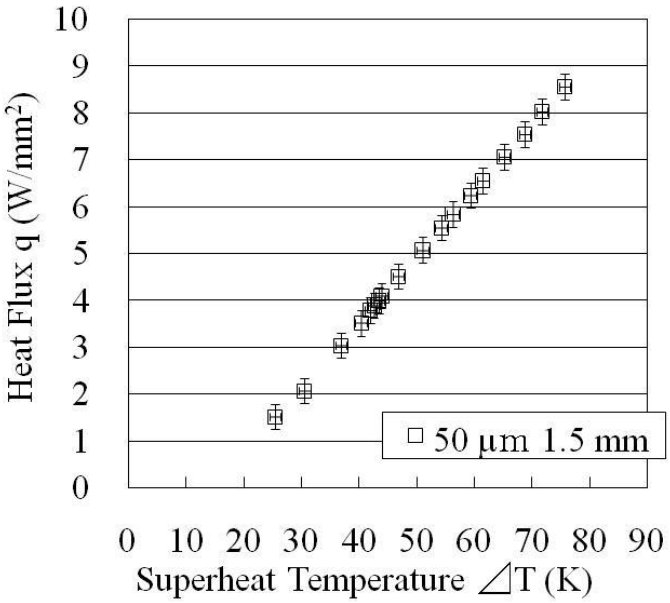

Fig. 8 Thermal performance of the sintered copper evaporator. The maximum value of 8.5 W/mm^2 is not due to dryout, but instead damage to the heater lead wire.

Fig. 8 shows the thermal performance of a sintered copper powder evaporator. The particular test sample shown was able

to dissipate 8.5 W/mm^2. The testing was stopped when the heater lead wire burnt out when the heat flux reached 9 W/mm^2, and was not a dryout heat flux limitation. Additionally, this sample was charged with a large amount of fluid, specifically intended to accommodate operation at the highest heat flux; however, this leads to an increase in the thermal resistance at the intermediate fluxes.

A comparison of four different sintered copper evaporators is shown in Fig. 9. Each evaporator has a different copper particle diameter and layer thickness combination. Smaller-diameter particles would be expected to increase the evaporation meniscus area per unit area of the substrate.

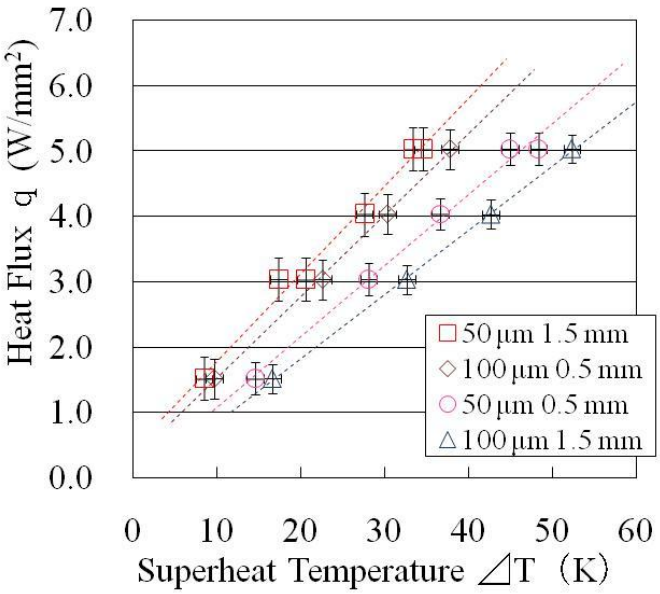

Fig. 9 Comparison of the thermal performance of four different sintered copper evaporators.

For a 0.5 mm wick thickness, the larger diameter particles (100 μm) lead to a lower superheat than the smaller (50 μm diameter) particles. The improved performance for the larger particles is likely related to the increased effective thermal conductivity of this sample. The ligaments formed due to sintering between neighboring 50 μm diameter particles had a diameter of approximately 20 μm as observed from SEM images, and are smaller than those formed for the 100 μm diameter particles, approximately 27 μm. This difference in connectedness of neighboring particles could imply a lower thermal conductivity for the smaller particles, causing the measured superheat temperature of the 50 μm sintered sample to be larger.

With the particle diameter fixed at 100 μm, the superheat with the 0.5 mm thickness sample is smaller than with the thicker (1.5 mm) sample. While this could be related simply to the added material thermal resistance of the thicker sample, it could also be due to the permeability difference between the fabricated samples. The ligament diameters in the 1.5 mm thick sample are observed to be larger than those in the 0.5 mm thick sample, possibly because of the greater settling of the thicker layer of particles during the sintering process. This increased ligament diameter reduces the open area for fluid flow within the wick leading to a lower permeability, and could explain the larger superheat temperatures for the 1.5 mm sintered sample at a given heat flux.

It is likely that an optimum solution exists for maximum thermal performance in terms of the extent of sintering (and therefore, the ligament diameter). At zero sintering, the thermal conductivity is poor, while excessive sintering is a detriment to the permeability.

Effects of CNT Parameters

Details of the preparation and characterization of three different configurations of microstructures with CNT coatings are first discussed. The microstructures considered are as follows:

- 50 μm particle diameter and 0.5 mm wick thickness
- 100 μm particle diameter and 0.5 mm wick thickness
- 50 μm particle diameter and 1.5 mm wick thickness

CNT-coated (nano-structured) sintered copper particles of 50 μm diameter in a 0.5 mm thick layer are shown in Fig. 10 and Fig. 11. The CNTs are grown in Fig.10 by sputtering, while the sample in Fig. 11 is prepared by using the dendrimer catalyst. Table 1 contains a summary of the measured characteristics obtained from SEM images of the multi-walled CNTs grown on the samples. The sputtering process produces CNTs of lengths 20-25 μm and diameters 50-100 μm. Growth with the dendrimer catalyst resulted in a similar diameter but with a much shorter length, on the order of 1 μm. In addition, the number density of the CNTs grown by the sputtering process is four times greater than with the dendrimer catalyst process.

It is also noted that the dendrimer-grown sample retained some deposits of a foreign substance on the surface, which may have been pyrolysis residue that did not completely burn.

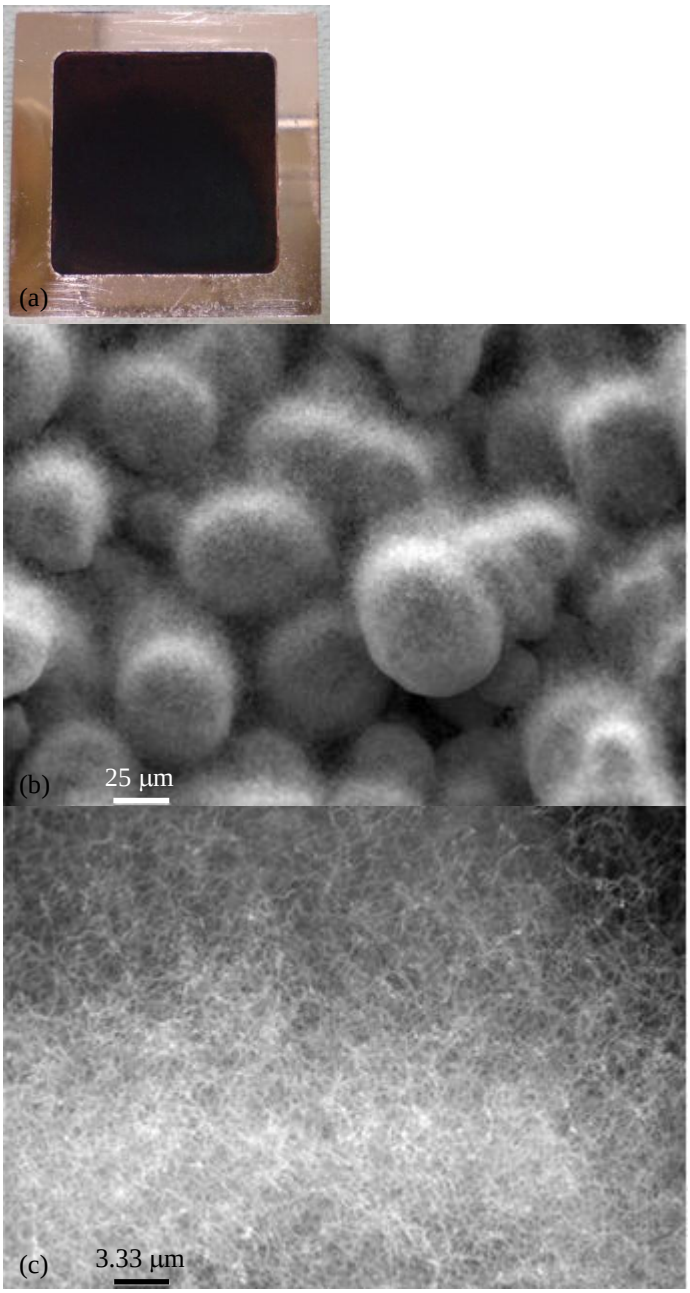

Fig. 10 CNT-coated sintered copper evaporator (50 μm diameter particles, layer thickness 0.5 mm, catalyst prepared by sputtering): (a) photograph of evaporator, (b) SEM image of this sample, and (c) SEM image (magnified).

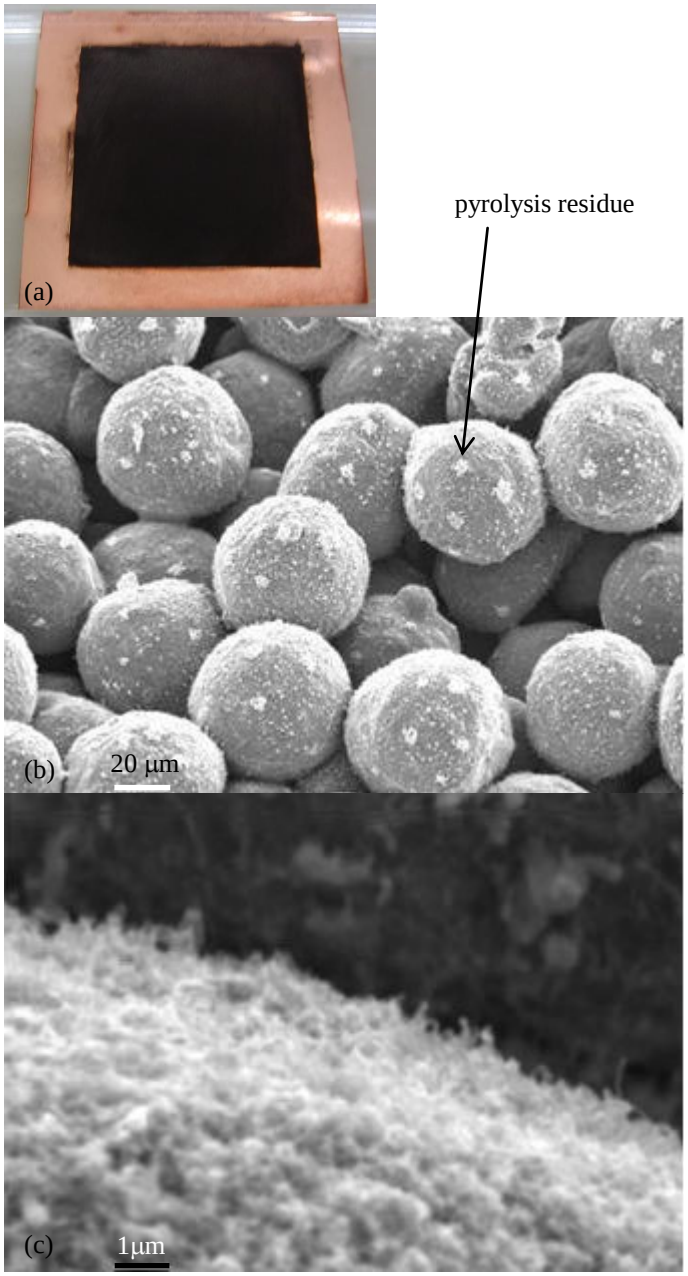

Fig. 11 CNT-coated sintered copper evaporator (50 μm diameter particles, 0.5 mm layer thickness, dendrimer catalyst): (a) photograph of evaporator sample, (b) SEM image of this sample, and (c) SEM image (magnified).

Table 1. Characteristics of CNTs grown on sintered Cu (50 μm diameter, 0.5 mm layer thickness).

	Length (μm)	Diameter (nm)	Density ($1/cm^2$)
sputtering	20-25	50-100	$20\text{-}40\times10^9$
dendrimer	1	100	$4\text{-}10\times10^9$

Fig. 12 shows the thermal performance results of the nano-structured 50 μm diameter sintered copper sample. The CNT-coated evaporators clearly result in better performance in terms of thermal resistance than the bare sintered copper powder evaporator; however, the added benefit with the dendrimer catalyst-grown CNTs over the bare sample is modest. The differences in performance between the two catalyst preparations for the CNT-coated evaporators are attributed to the large differences in the length and density that result from the different growth methods. Longer and denser CNTs may enhance the evaporation by providing a larger surface area.

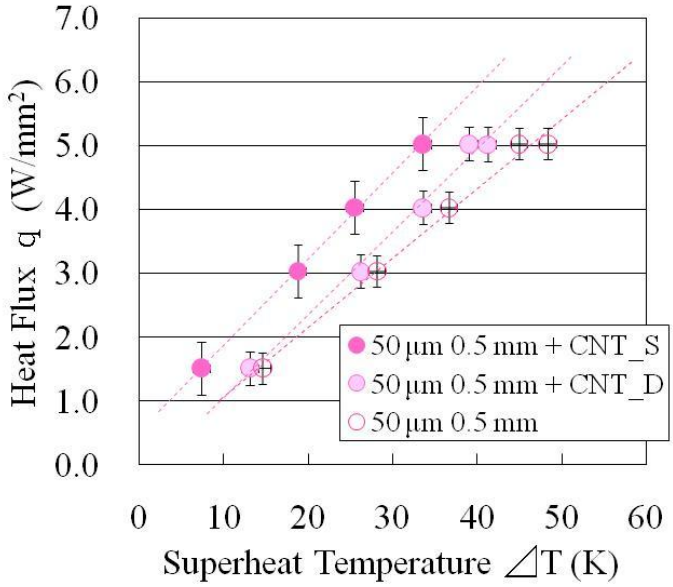

Fig. 12 Comparison between CNT-coated and bare sintered copper powder evaporators. The base sintered copper powder used for all samples is 0.5 mm thick and consists of 50 μm diameter particles.

Fig. 13 and Fig. 14 show details of the CNT-coated (nano-structured) sintered copper particles of a larger diameter than considered above – 100 μm diameter particles with 0.5 mm layer thickness – where the CNTs are grown using the two different approaches. Table 2 summarizes the characteristics of these samples.

The corresponding experimental results for thermal performance of these two samples, as compared to a bare sintered sample are shown in Fig. 15. The evaporator with CNTs coated CNT using a sputtered catalyst exhibits a lower thermal resistance than the bare sintered sample (except at the lowest heat flux). The CNT-coated sample prepared using a dendrimer catalyst, in contrast, shows degraded performance compared to the bare sample. As in the case of the experiments with the smaller particle diameter discussed above, these performance differences may be attributed to differences in the length and density of the CNTs grown by the two methods, as well as the amount of pyrolysis residue that is left over.

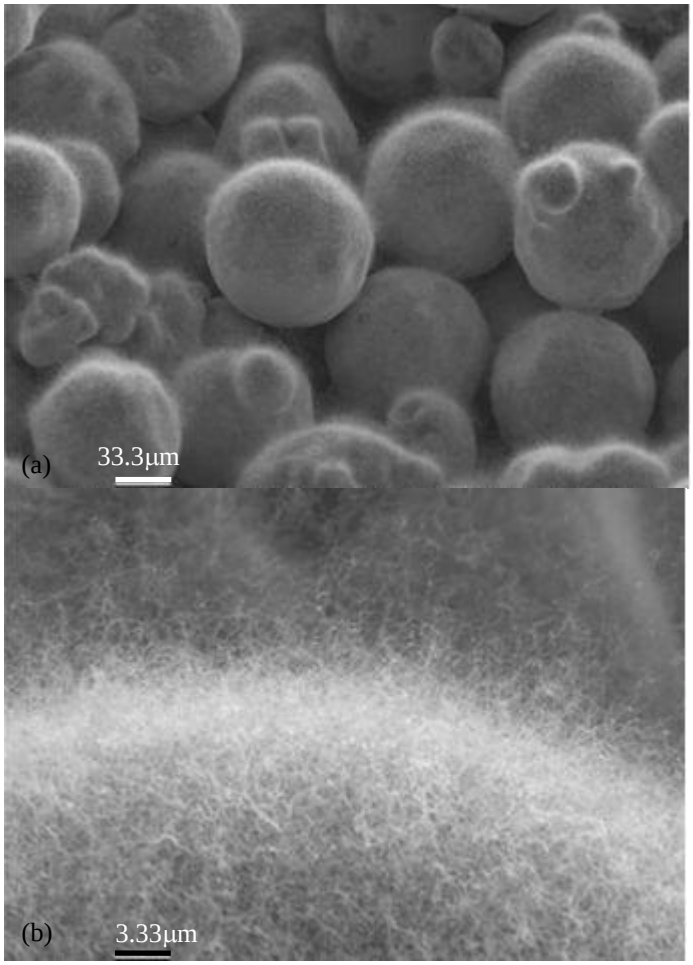

Fig. 13 CNT-coated sintered copper with particle diameter 100 μm and layer thickness 0.5 mm. The catalyst is prepared by sputtering. (a) SEM image of the evaporator, and (b) magnified SEM image.

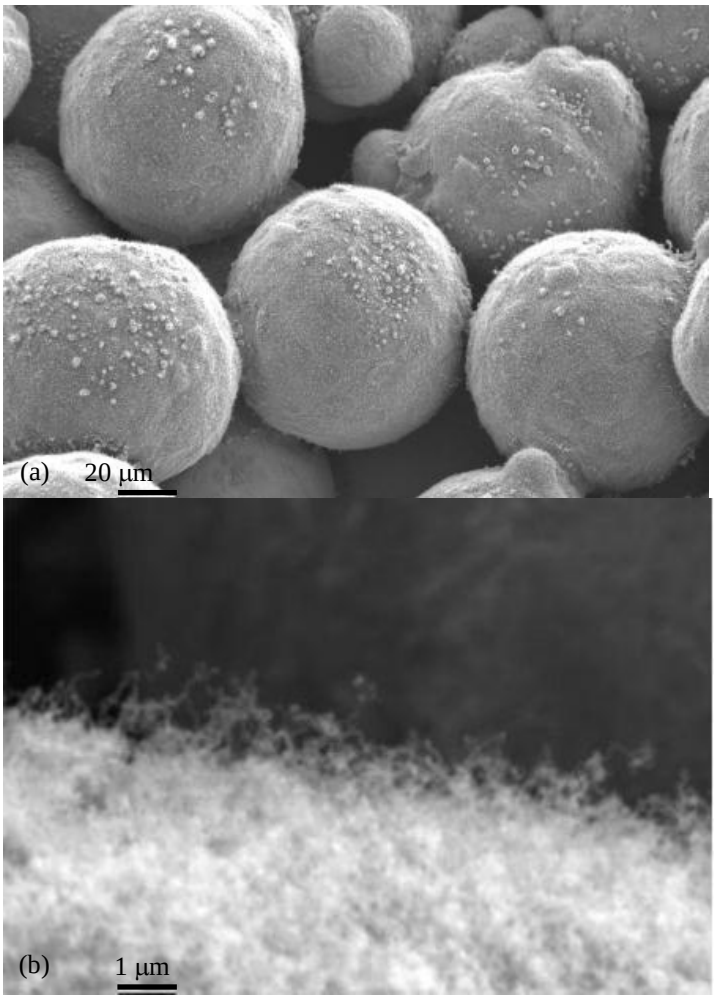

Fig. 14 CNT-coated sintered copper evaporator with particle diameter 100 μm and layer thickness 0.5 mm. The sample is prepared using a dendrimer catalyst. (a) SEM image of the evaporator, and (b) magnified SEM image.

Table 2. Characteristics of CNTs grown on sintered Cu (100 μm diameter, 0.5 mm layer thickness).

	Length (μm)	Diameter (nm)	Density ($1/cm^2$)
sputtering	10	50-100	$20\text{-}40\times10^9$
dendrimer	2.5	100	$4\text{-}10\times10^9$

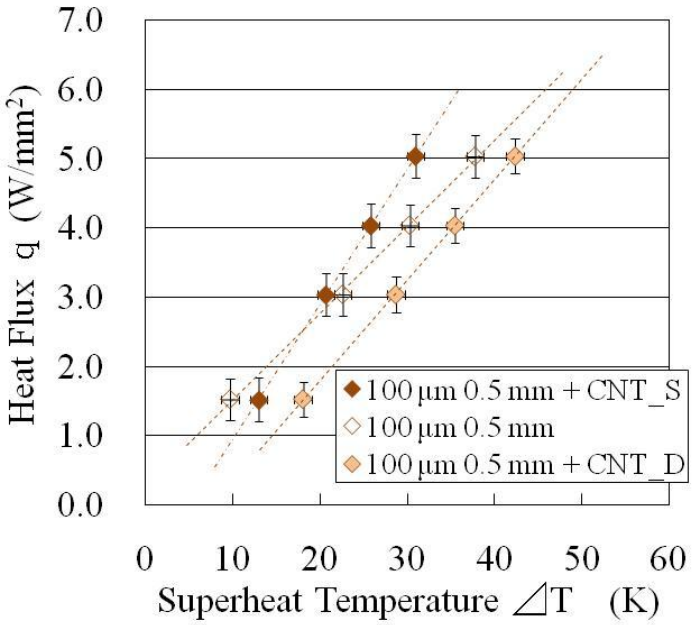

Fig. 15 Comparison between the CNT-coated and bare sintered powder evaporators. For all samples the base sintered copper powder has 100 μm diameter particles and is 0.5 mm thick.

Fig. 16 shows SEM images of a CNT-coated sintered copper sample with particle diameter 50 μm thickness 1.5 mm. This CNT-coating is prepared by using a dendrimer catalyst. Table 3 shows the characteristics of these CNTs. The multi-walled CNTs were estimated to be 0.5-1 μm long and 100 μm in diameter. The length of these CNTs is the shortest in our experiments. The density is also the lowest.

Experimental results for this sample are shown in Fig. 17.. The dendrimer based CNT-coated sample again performs worse than the bare sintered copper powder sample. As shown in Table 3, the CNTs in this case are very short and of low density. As observed in the previous results, the shorter, lower-density dendrimer-grown CNTs have worse, or at best similar, performance relative to the bare sintered powder counterparts. Further careful studies need to be conducted to understand the precise reasons for such behavior.

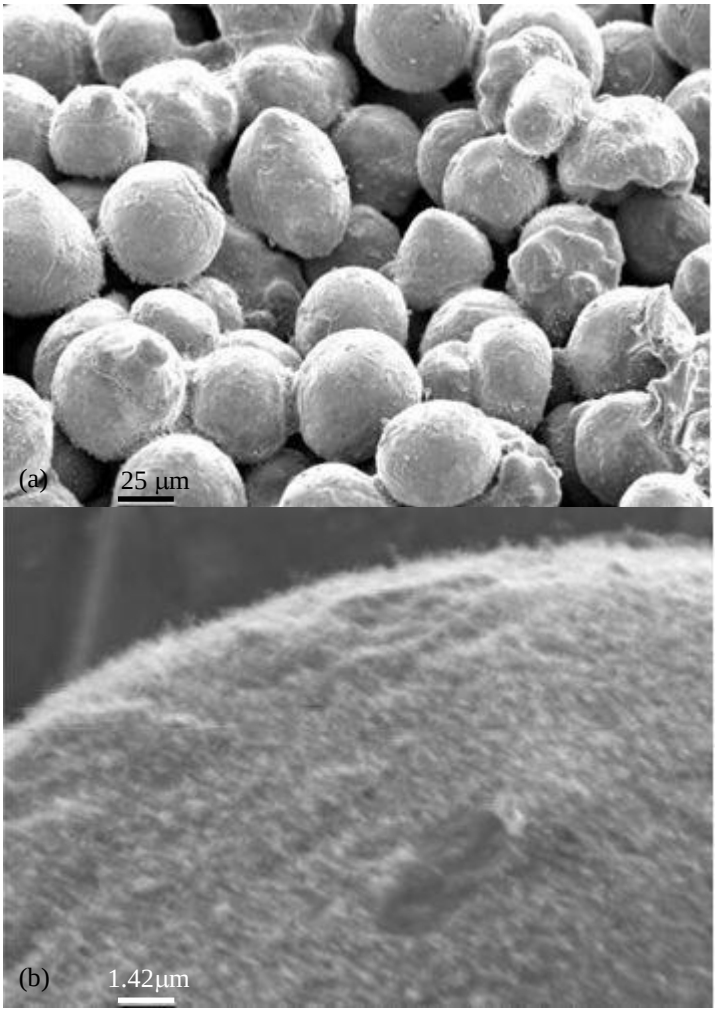

Fig. 16 CNT-coated sintered copper sample with particle diameter 50 μm and layer thickness 1.5 mm, prepared using a dendrimer catalyst. (a) SEM image of the sample, and (b) magnified SEM image.

Table 3. Characteristics of CNTs grown on sintered Cu (50 μm particle, 1.5 mm layer thickness).

	Length (μm)	Diameter (nm)	Density (1/cm^2)
dendrimer	0.5-1	100	0.4-1×10^9

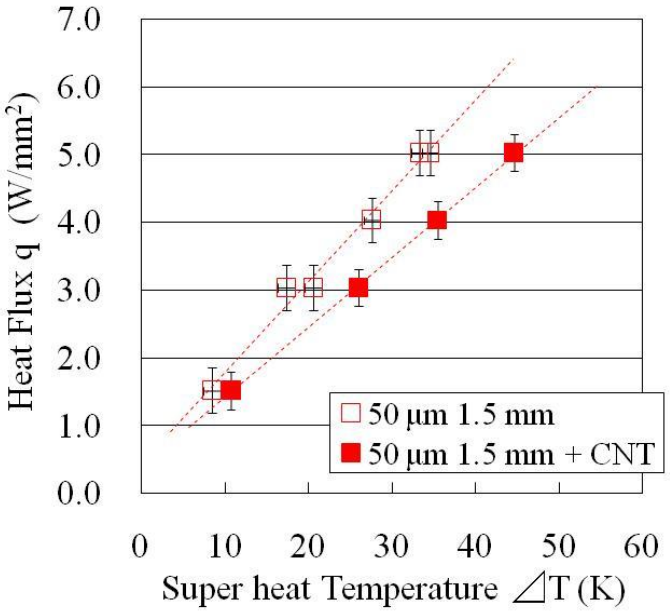

Fig. 17 Comparison of thermal performance between the CNT-coated and bare sintered powder samples. For both samples the base sintered copper powder has 50 μm diameter particles and is 1.5 mm thick.

Thermal Resistances of the Different Samples

Table 4 summarizes the thermal resistances of all the evaporator substrates investigated. These thermal resistances are based on an input heat flux of 5 W/ mm^2. Nano-structured samples produced by sputtering tend to show improved performance compared to the bare sintered copper powder with a thermal resistance decrease of up to 37%. The samples prepared by using dendrimer did not exhibit a similar ability to reduce thermal resistance.

Table 4. Comparison of thermal resistances of the different samples, based upon the thermal resistance at 5 W/mm^2. The best performing sample has a thermal resistance of 0.25 K/W corresponding to a particle size of 100 μm and a 0.5 mm layer thickness.

particle size, layer thickness, catalyst for CNT growth	K/W
100 μm, 0.5 mm, sputtering	0.25
50 μm, 0.5 mm, sputtering	0.27
50 μm, 1.5 mm, bare	0.27
100 μm, 0.5 mm, bare	0.30
50 μm, 0.5 mm, dendrimer	0.31
100 μm, 0.5 mm, dendrimer	0.34
50 μm, 1.5 mm, dendrimer	0.36
50 μm, 0.5 mm, bare	0.37
100 μm, 1.5 mm, bare	0.42

CONCLUSIONS

A passive, two-phase heat spreader is developed for ultra-high heat flux applications. Evaporator surfaces with CNT nanostructured layers grown on top of the surface of sintered copper particle micro-structures were fabricated and characterized. A thermal CVD method is used for fabrication of the CNTs and UV irradiation is utilized to functionalize the surfaces to render them hydrophilic. The density and length of CNT arrays are varied by means of the use of two different catalysts – sputtered layers and dendrimer. The results of this experimental investigation reveal that the heat spreader developed can dissipate at least 8.5 W/mm^2 when using a micro-structured sintered particle wick evaporator. Further, nano-structuring the sintered particles with CNTs are shown to hold the potential for additional reductions in thermal resistance. Reductions in thermal resistance of up to 20-37% with CNT nanostructuring relative to a bare sintered surface were demonstrated. The different catalyst growth methods were found to yield differing CNT lengths and densities which directly impact the observed thermal performance.

NOMENCLATURE

A	cross-sectional area, m^2
K	permeability, m^2
L	length, m
$\dot{m}$	mass flux, kg/s
ΔP	pressure differential, Pa
r_{eff}	effective radius, m

Greek symbols

μ	viscosity, Pa s
ρ	mass density, kg/m^3
σ	surface tension coefficient, N/m
θ	contact angle

Subscripts

cap	capillary
con	condenser
eva	evaporator
l	liquid

ACKNOWLEDGMENTS

The authors express their gratitude to Prof. Tim Fisher, Prof. Jayathi Murthy, Ram Ranjan, and Glen Powell of Purdue University and Dr. Yuichi Ishida of Sony for their support of this study.

REFERENCES

(1) http://www.fujikura.co.jp/00/news/0310/news2.html

(2) Zhao, Y. and Chen, C., 2007, "Vaporization Heat Transfer in Sintered Copper Wicks with Micro-grooves in Heat Pipe Evaporators," Thermal Challenges in Next Generation Electric Systems THERMES 2007, Millpress, pp. 241-247

(3) Zhao, Y. and Chen, C., 2006, "An Investigation of Evaporation Heat Transfer in Sintered Copper Wicks With Microgrooves," Proceedings of IMECE2006, Chicago

(4) Li, C. and Peterson, G. P., 2006, "Comprehensive Comparisons between Evaporation and Pool Boiling on Thin Micro Porous Coated Surfaces," Proceedings of IMECE2006, Chicago

(5) Li, C., Peterson, G. P. and Wang, Y., 2006, "Evaporation/Boiling in Thin Capillary Wicks- Wick Thickness Effects," ASME Journal of Heat Transfer, 128, pp.1312-1319

(6) Li, C. and Peterson, G. P., 2006, "Evaporation/Boiling in Thin Capillary Wicks-Effects of Volumetric Porosity and Mesh Size," ASME Journal of Heat Transfer, 128, pp.1320-1328

(7) Hasebe, S., Shikazono, N. and Kasagi, N., 2004, "Modeling and Design of Micro Groove Falling Film Evaporators," ICMM2004, New York

(8) Wang, H., Garimella, S. V. and Murthy, J. Y., 2007, "Characteristics of an Evaporating Thin Film in a Microchannel," International Journal of Heat and Mass Transfer, 50, pp.3933-3942

(9) Wang, J. and Catton, I., 2001, "Enhanced Evaporation Heat Transfer in Triangular Grooves Covered with a Thin Fine Porous Layer," Applied Thermal Engineering, 21, pp.1721-1737

(10) Mughal, M. P. and Plumb, O. A., 1996, "An Experimental Study of Boiling on a Wicked Surface," International Journal of Heat and Mass Transfer, 39, pp.771-777

(11) Semenic, T., Lin, Y. and Catton, I., 2005, "Biporous Sintered Copper for a Closed Loop Heat Pipe Evaporator," Proceedings of IMECE2005, Orlando

(12) Abhat, A. and Seban, R. A., 1974, "Boiling and Evaporation from Heat Pipe Wicks With Water and Acetone," Journal of Heat Transfer, 96, pp.331-337

(13) Nakayama, W., Daikoku, T., Kuwahara, H. and Nakajima, T., 1980, "Dynamic Model of Enhanced Boiling Heat Transfer in porous Surfaces Part 1: Experimental Investigation," Journal of Heat Transfer, 102, pp.445-450

(14) Vityaz, P. A., Konev, S. V., Medvedev, V. B. and Sheleg, V. K., 1984, "Heat Pipes with Bidispersed Capillary Structures," Proceedings of 5th International Heat Pipe Conference, Part 1, Tsukuba

(15) Iverson, B. D., Davis, T. W., Garimella, S. V. and North, M. T., 2007, "Heat and Mass Transport in Heat Pipe Wick Structures," Journal of Thermophysics and Heat Transfer, 21, pp.392-404

(16) North, M. T., Sarraf, D. B., Maidanik, Y. F. and Vershinin, S., 1997, "High Heat Flux Loop Heat Pipes," 6th European Symposium on Space Environmental Control Systems, Netherlands

(17) Liter, S. G. and Kaviany, M., 2001, "Pool-Boiling CHF Enhancement by Modulated Porous-Layer Coating: Theory and Experiment," International Journal of Heat and Mass Transfer, 44, pp.4287-4311
(18) Launay, S., Fedorov, A. G., Joshi, Y., Cao, A. and Ajayan, P. M., 2006, "Hybrid Micro-nano Structured Thermal Interfaces for Pool Boiling Heat Transfer Enhancement," Microelectronics Journal, 37, pp.1158-1164
(19) Ahn, H. S., Sinha, N., Zhang, M. and Baughman, R. H. 2006, "Pool Boiling Experiments on Multiwalled Carbon Nanotube (MWCNT) Forests," Journal of Heat Transfer, 128, pp.1335-1342
(20) Ujereh, S., Fisher, T. S. and Mudawar, I., 2007, "Effects of Carbon Nanotube Arrays on Nucleate Pool Boiling," International Journal of Heat and Mass Transfer, 50, pp. 4023-4038
(21) Ujereh, S., Mudawar, I., Amama, P. B. and Fisher, T. S., 2005, "Enhanced Pool Boiling Using Carbon Nanotube Arrays on a Silicon Surface," Proceedings of IMECE 2005, pp.691-696
(22) Cai, Q., Zhao, Y., Tsai, C., and Chen C., 2009, "Investigation of High Heat Flux Cooling Using Carbon Nanotube Bi-wick Structure and Integrated Platinum Thermometer /Heater," Proceedings of the ASME 2009 Heat Transfer Summer Conference
(23) Hashimoto, M., Yazawa, K., Weibel, A. J. and Garimella, S. V., 2010, "A Two-phase Heat Spreader for Cooling High Heat Flux Sources," Proceedings of ITherm 2010 (in Press)
(24) Faghri, A., 1995, "Heat Pipe Science and Technology," Taylor& Francis, pp. 123-141
(25) Dunn, P. D. and Reay, D. A., 1994, "Heat Pipes," Fourth Edition Pergamon, pp. 172-173
(26) Amama, P. B., Cola, B. A., Sands, T. D. and Fisher, T. S., 2007, "Dendrimer-assisted Controlled Growth of Carbon Nanotubes for Enhanced Thermal Interface Conductance," Nanotechnology, 18
(27) Amama, P. B., Ogebute, O., Maschmann, M. R. and Fisher, T. S., 2006, "Dendrimer-assisted Low-temperature Growth of Carbon Nanotubes by Plasma-Enhanced Chemical Vapor Deposition," Chemical Communications, pp.2899-2901
(28) Asano, K., Kondo, D., Kawabata, A. and Awano, Y., 2006, "Chemical Modification of Multiwalled Carbon Nanotubes by Vacuum Ultraviolet Irradiation Dry Process," Japanese Journal of Applied Physics, 45, 4B, pp.3573-3576